Bio-nanotechnology

DOI: 10.1002/anie.201106180

Multifunctional Mesoporous Composite Nanocapsules for Highly Efficient MRI-Guided High-Intensity Focused Ultrasound Cancer Surgery**

Yu Chen, Hangrong Chen, Yang Sun, Yuanyi Zheng, Deping Zeng, Faqi Li, Shengjian Zhang, Xia Wang, Kun Zhang, Ming Ma, Qianjun He, Linlin Zhang, and Jianlin Shi**

As a representative "bloodless surgical knife", high-intensity focused ultrasound (HIFU) surgery is becoming one of the most promising noninvasive and nonradiative transcutaneous treatment protocols for cancer therapy.[1] Theoretically, HIFU focuses the ultrasound waves produced outside the body on in vivo lesions (therapeutic targets), because ultrasonic energy can penetrate tissue and deposit energy thereby inducing mechanical, thermal, and cavitation effects in the targeted tissues and destroying the tumor vasculature and simultaneously causing coagulative necrosis of cancer cells.[2] However, two typical challenges must be overcome prior to extensive clinical application. One is how to realize the accurate positioning of therapeutic targets for focused ultrasound by clinical imaging protocols to ensure complete eradication of microscopic tumor foci, and the other is how to achieve the highly efficient HIFU therapy under simultaneous imaging guidance.[1b] As an alternative to expensive equipment upgrades, recently developed nano-biotechnology may provide highly efficient and low-cost pathways to solve these two problems.

Typically, real-time diagnostic ultrasound (US) and magnetic resonance imaging (MRI) are now the two representative imaging and diagnosis modalities for imaging-guided HIFU surgery.[1b,3] MRI shows advantages over US, because it combines the merits of noninvasive diagnosis mode, excellent spatial and anatomical resolution, and the capacity of quantitative evaluation of disease pathogenesis.[4] Unfortunately, conventional MRI-guided HIFU still suffers from unsatisfactory imaging and guidance effects and relatively low HIFU therapeutic efficiency. Herein we report, as a proof of concept, on nanosized multifunctional HIFU synergistic agents (SAs) for cancer surgery based on novel mesoporous composite nanocapsules (MCNCs), which also function as the contrast agents (CAs) for MRI-guided accurate location of the therapeutic focusing spot in the targeted tumor tissue. Although gadolinium(III)-based molecular chelates have been widely adopted in the current clinical disease diagnosis, the U.S. Food and Drug Administration warns that Gd^{3+}-based CAs are associated with nephrogenic systemic fibrosis in patients with impaired kidney function, hypersensitivity reactions, and nephrogenic fibrosing dermopathy.[5] Searching for alternatives to Gd^{3+} chelates has thus been at the forefront of recent research. In keeping with this trend, we chose another important family of T_1 CAs for MRI: manganese-based nanoparticulate systems, in which manganese oxide species were evenly distributed within the pore network of MCNCs. The unique nanostructural characteristics of MCNCs combine the merits of highly dispersed manganese oxide species confined within mesopores for efficient T_1-weighted MRI with large hollow interiors for the encapsulation and delivery of guest molecules for active HIFU therapy.

The design process and microstructure of MCNCs are shown in Scheme 1. Monodispersed hollow mesoporous silica nanocapsules were chosen for further decoration with manganese species. The silica nanocapsules were fabricated by a combined soft/hard double-templating strategy based on selective etching of different structural features (Figure S1 in the Supporting Information).[6] The mesopores are directed by surfactant micelles (soft template), while the hollow interiors are templated by monodispersed silica cores (hard template). The organic micelles formed by the self-assembly of quaternary cationic surfactants (cetyltrimethyl ammonium bromide, C_{16}TAB) are uniformly located within the meso-

[*] Dr. Y. Chen, Prof. Dr. H. Chen, Dr. X. Wang, Dr. K. Zhang, Dr. M. Ma, Dr. Q. He, Dr. L. Zhang, Prof. Dr. J. Shi
State Laboratory of High Performance Ceramic and Superfine Microstructure, Shanghai Institute of Ceramics
Chinese Academy of Sciences
Shanghai, 200050 (P.R. China)
E-mail: jlshi@sunm.shcnc.ac.cn
hrchen@mail.sic.ac.cn

Dr. Y. Sun, Prof. Dr. Y. Zheng
Second Affiliated Hospital of Chongqing Medical University
Chongqing, 400010 (P.R. China)

Prof. Dr. D. Zeng, Prof. Dr. F. Li
State Key Laboratory of Ultrasound Engineering in Medicine Co-founded by Chongqing and the Ministry of Science and Technology
Chongqing Key Laboratory of Ultrasound in Medicine and Engineering, College of Biomedical Engineering
Chongqing Medical University, Chongqing, 400016 (P.R. China)

Dr. S. Zhang
Department of Radiology, Cancer Hospital/Institute & Department of Oncology, Shanghai Medical College, Fudan University
Shanghai, 200032 (P.R. China)

[**] MRI = magnetic resonance imaging. This work was supported by the National Basic Research Program of China (973 Program, Grant No. 2011CB707905), Shanghai Rising-Star Program (Grant No. 10QH1402800), National Nature Science Foundation of China (Grant No. 51132009, 50823007, 50972154, 51072212, 51102259), the Science Foundation for Youth Scholar of State Key Laboratory of High Performance Ceramics and Superfine Microstructures (Grant No. SKL201001), CASKJCX Projects (Grant No. KJCX2-YW-210) and the Science and Technology Commission of Shanghai (Grant No. 10430712800, 10QH1402800).

Supporting information for this article is available on the WWW under http://dx.doi.org/10.1002/anie.201106180.

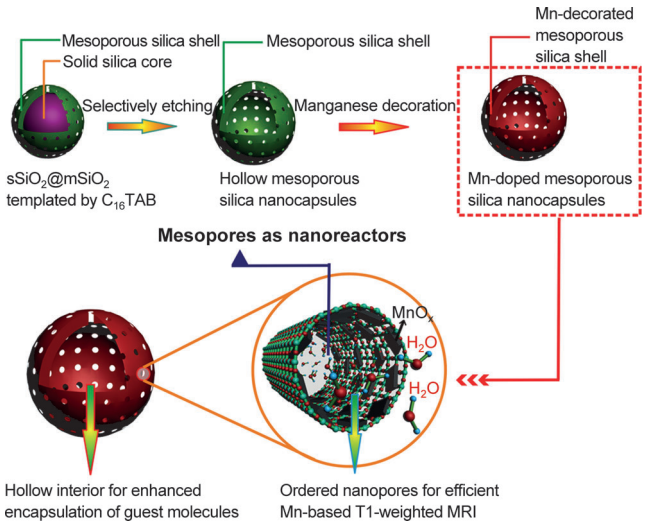

Scheme 1. Schematic diagram of the synthetic procedure for MCNCs and their corresponding microstructures.

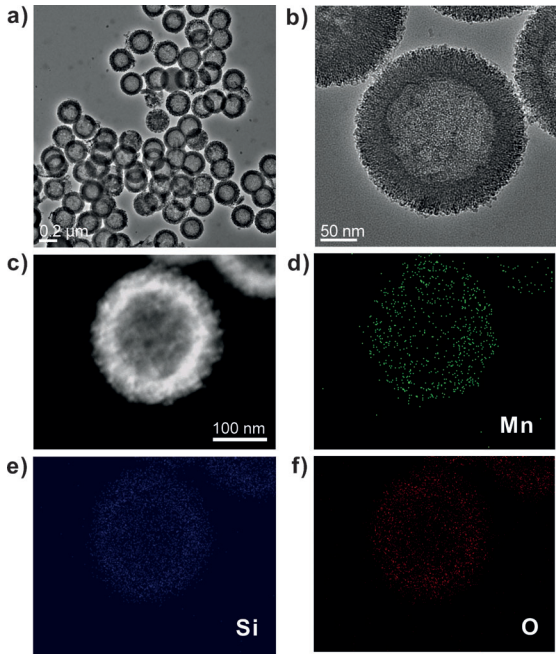

Figure 1. a,b) TEM images, c) dark-field STEM (scanning transmission electron microscopy) image, and d–f) corresponding element mapping (Mn, Si, and O, respectively) of MCNCs.

pores. When strongly oxidizing MnO_4^- ions are introduced, they can react with C_{16}TAB molecules to generate manganese oxide nanoparticles in situ within the mesopore network. The mesopore channels function as nanoreactors, where the redox reaction takes place. Therefore, the formed manganese oxide nanoparticles are highly dispersed within the mesoporous structure. This structural characteristic is highly beneficial for T_1-weighted MRI, because the large surface area and tunable pore sizes of the MCNCs ensure high dispersity of manganese oxide species and free diffusion of water molecules within the mesopores, thus resulting in greatly enhanced water accessibility of the manganese paramagnetic centers and therefore in the much-improved MRI efficacy.[7] The valence of manganese species can be controlled by heating under reducing atmosphere (e.g. H_2/Ar), thereby allowing modulation of the MRI capability of MCNCs. Moreover, the large hollow interior and well-defined mesopore structure of MCNCs guarantees efficient encapsulation and delivery of guest molecules.[6a,b,8]

Figure 1 shows the morphology, structural, and chemical characteristics of MCNCs. The hollow nanostructure of MCNCs can be directly demonstrated by the contrast differences between the core and shell in TEM images (Figure 1 a, b). The average hydrated-particulate size of MCNCs measured by dynamic light scattering (DLS) was 342 nm (Figure S2 in the Supporting Information). Energy-dispersive X-ray spectroscopy (EDS) element mapping of Mn, Si, and O was conducted to investigate the distribution of manganese paramagnetic centers within the mesopores (Figure 1 c–f). Manganese was well-distributed in the whole hollow mesoporous silica matrix without apparent accumulation on the particle surface owing to the formation and deposition of manganese oxide species within the mesopores. Inductively coupled plasma atomic emission spectroscopy (ICP-AES) results showed that the manganese content in MCNCs was 6.4%. The structural characteristics of the pores were determined by the typical N_2 adsorption–desorption technique. The mesopores are well-defined with a surface area of 468 $m^2 g^{-1}$, a pore volume of 0.6 $cm^3 g^{-1}$, and hierarchical pore sizes of 3.8 and 12.6 nm (Figure S3 in the Supporting Information), thus suggesting that the mesoporous systems of the MCNCs remain open and penetrable after the decoration with manganese oxide nanoparticles, which guarantees the further efficient encapsulation and delivery of guest molecules.[6a,b,8]

The first assessment of the MCNCs as CAs for MRI was conducted in aqueous solution using a 3.0 T human clinical MR scanner. The longitudinal relaxation rate (T_1^{-1}) and transverse relaxation rate (T_2^{-1}) as a function of the manganese ion concentrations in the MCNCs before and after H_2/Ar reduction were investigated (Figure S4 in the Supporting Information). The MCNCs have relaxation rates $r_1 = 0.57\ mM^{-1}s^{-1}$ and $r_2 = 19.9\ mM^{-1}s^{-1}$ before the H_2/Ar treatment. However, r_1 and r_2 of the MCNCs after H_2/Ar treatment increased to 1.84 and 42.0 $mM^{-1}s^{-1}$, respectively, and are thus 3.2 and 2.1 times higher than their original values before H_2/Ar reduction. The increased relaxivities are attributed to the decreased valence of manganese under reducing atmosphere, which was supported further by the change in electron spin resonance (ESR) spectra of MCNCs before and after H_2/Ar treatment (Figure S5 in the Supporting Information). This r_1 value (1.84 $mM^{-1}s^{-1}$) is 4.0, 9.2, 13.2, and 14.3 times higher than those of 7 nm (0.37 $mM^{-1}s^{-1}$), 15 nm (0.18 $mM^{-1}s^{-1}$), 20 nm (0.13 $mM^{-1}s^{-1}$), and 25 nm (0.12 $mM^{-1}s^{-1}$) monodispersed MnO nanoparticles, respectively.[9] The effects of MCNCs on decreasing the longitudinal relaxation time (T_1) and the transverse relaxation time (T_2) of hydrogen protons in aqueous solution were further illustrated by changes of the signal intensities with increasing manganese-ion concentrations (Tables S1 and S2 in the Supporting

Information). Note that the specific relaxivity of MCNCs was also substantially higher than that of silica-coated or mesoporous-silica-coated hollow or solid manganese oxide nanoparticles (MnO@SiO_2, Mn_3O_4@SiO_2, MnO@mSiO_2, and hMnO@mSiO_2), because the silica coatings introduced after manganese oxide nanoparticle synthesis would partially shield the paramagnetic manganese centers entrapped within the core, thus resulting in significantly reduced chances of interactions with water molecules.[9,10] The pore-channel system in such MCNCs is responsible for the high dispersity of manganese paramagnetic centers and facilitates fast diffusion of water molecules inside the mesopore network, causing substantially enhanced relaxivity of manganese-based T_1 CAs for MRI.

The uptake of MCNCs by cancer cells was demonstrated by in vitro confocal laser scanning microscopy (Figure S6 in the Supporting Information), which suggests that they will be effective for further in vivo MRI-guided HIFU cancer surgery. Furthermore, it is known that passive targeting based on the enhanced permeability and retention (EPR) effect of tumors is beneficial for tumor-selective drug delivery, which can be used to target organs with large amounts of resident macrophages, such as liver and spleen.[11] In this respect, we chose the VX2 liver tumor model in rabbits for the systematic evaluation of the effectiveness of MCNCs for MRI-guided HIFU cancer surgery. Furthermore, to achieve the highly efficient synergistic effect of MCNCs for HIFU, we encapsulated biocompatible perfluorohexane (PFH) molecules into MCNCs by making use of the nanocapsules' large hollow interiors and penetrable mesoporous structures. PFH has a relatively low boiling point (51–59 °C), which lets it easily gasify and generate bubbles when heat is generated by HIFU exposure.[12] The T_1-weighted MR images show that the signals of liver increase significantly in the prolonged time course after the administration of either MCNCs/PBS or PFH-MCNCs/PBS (Figure 2 b_1–b_4 and Figure 2 c_1–c_4), while the administration of PBS does not lead to signal enhancement in the time course studied (Figure 2 a_1–a_4). The liver-signal enhancement is mainly due to phagocytosis of MCNCs by the reticuloendothelial systems (RES) mentioned above, thus showing that passive targeting occurs. The MRI signals of normal liver tissue increase more than those of the tumor tissue, leading to much clearer margins between tumor and normal tissue. This effect is very beneficial for the subsequent HIFU surgery, because the high-quality MR images allow the ultrasound energy to be precisely focused on the desired tumor site, thus resulting in improved therapeutic efficiencies but substantially limited damages to normal tissues.

The effectiveness of MCNCs as the SAs for HIFU synergistic therapy was firstly evaluated ex vivo by choosing degassed bovine liver as the model tissue after the HIFU exposure with the SAs (MCNCs/PBS and PFH-MCNCs/PBS) or with PBS as the control. The real-time ultrasound imaging ex vivo was employed to monitor the whole assessment process. When a syringe with the agents was inserted into the bovine liver, the position of the needle tip was monitored by the ultrasound imaging. Immediately after the injection of different agents, focused ultrasound was applied on the injection site with the desired power and time durations

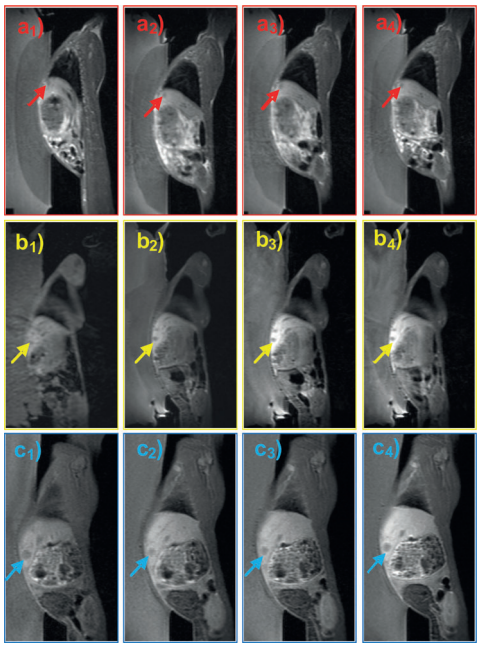

Figure 2. In vivo T_1-weighted MRI of rabbits bearing VX2 liver tumor before administration (a_1, b_1, and c_1) and 5 min (a_2, b_2, and c_2), 15 min (a_3, b_3, and c_3), and 30 min (a_4, b_4, and c_4) after administration of different agents (PBS: a_1–a_4; MCNCs/PBS: b_1–b_4; PFH-MCNCs/PBS: c_1–c_4) through the ear vein. PBS = phosphate-buffered saline. Arrows indicate the tumor.

(150 W, 5 s and 250 W, 5 s). The bovine liver was subsequently anatomized to calculate the damaged volume caused by HIFU exposure. As shown in Figure 3 a, the mean volume of the liver tissue coagulated by HIFU exposure varies significantly. The livers injected with MCNCs/PBS exhibited higher therapeutic efficacy than the blank control (PBS), implying that MCNCs alone could cause the synergistic effect in HIFU therapy. Importantly, the mean volume of coagulated liver tissue in the group that received PFH-MCNCs/PBS (150 W, 5 s 86.5 mm^3; 250 W, 5 s 153.1 mm^3) was distinctly larger than in the groups receiving PBS (150 W, 5 s 31.7 mm^3; 250 W, 5 s 66.6 mm^3) and MCNCs/PBS (150 W, 5 s 43.7 mm^3; 250 W, 5 s 109.3 mm^3). The ex vivo results showed that the MCNCs could efficiently encapsulate and deliver PFH molecules to remarkably enhance the therapeutic efficiency of HIFU. In the group that received PFH-MCNCs/PBS, the low exposure ultrasound power (150 W, 5 s 86.5 mm^3) caused a larger coagulated tissue volume than the high exposure ultrasound power (250 W, 5 s 66.6 mm^3) caused in the group receiving only PBS. This effect is very beneficial for HIFU therapy, because high ultrasound energy could damage the normal tissues in the acoustic propagation channels. Fortunately, the introduction of PFH-MCNCs/PBS as SAs for HIFU could reach enhanced therapeutic efficiency at much reduced exposure power input.

The integration of piezoelectric ultrasound transducers and MRI magnets makes the MRI-guided HIFU surgery technically feasible.[1b,3a,c] As shown in Figure 3 b, MRI is firstly conducted to locate the focused ultrasound in the targeted tumor tissue with the assistance of MCNCs as the

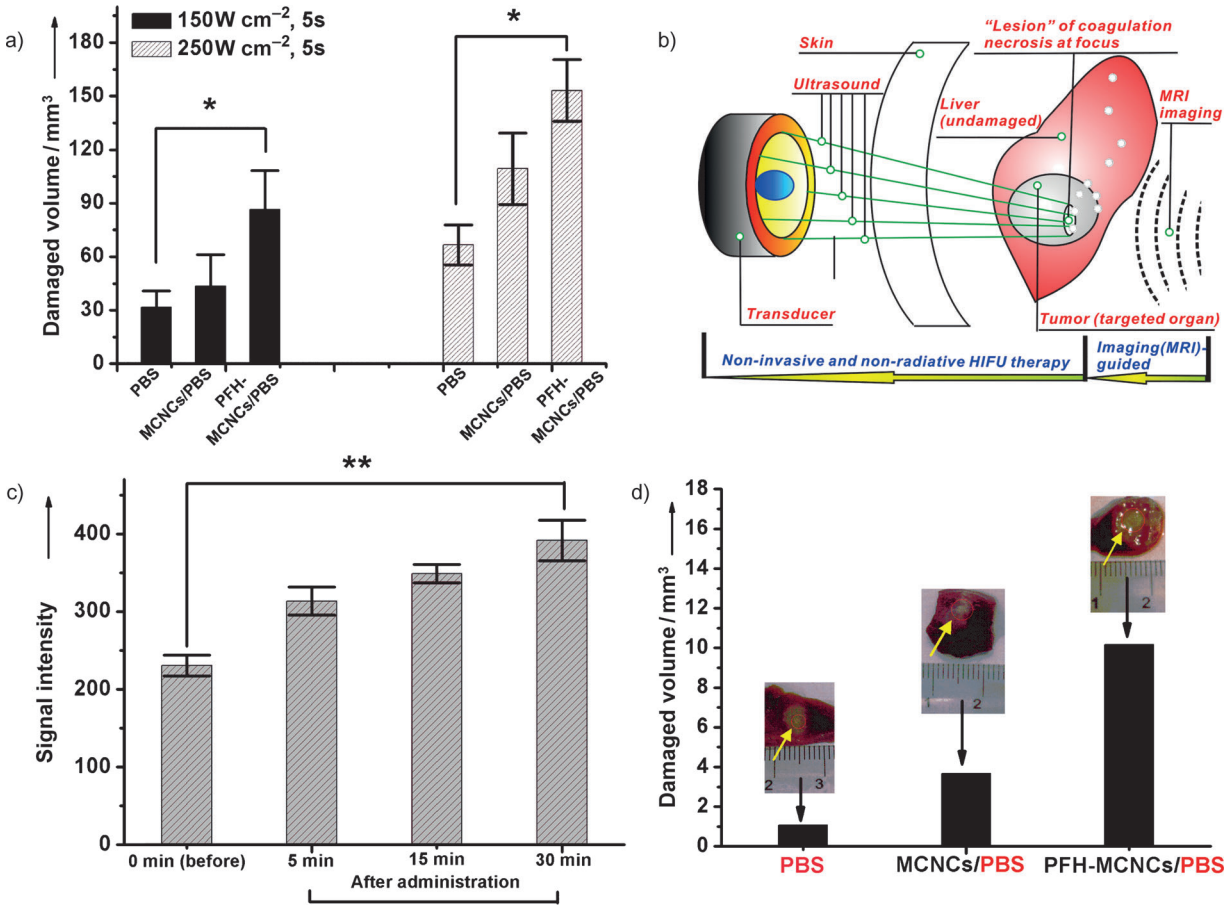

Figure 3. a) Coagulated-tissue volume of degassed bovine liver after intratissue injection of PBS (200 μL), MCNCs/PBS (200 μL), and PFH-MCNCs/PBS (200 μL) under the same irradiation power and duration (150 $W cm^{-2}$, 5 s and 250 $W cm^{-2}$, 5 s; $*P<0.05$). b) Technical principal of MRI-guided HIFU for the surgery of hepatic neoplasm in rabbits. c) T_1-weighted MRI signal intensities of tumor tissue before and after intravenous administration of PFH-MCNCs/PBS ($**P<0.005$). d) In vivo coagulated necrotic-tumor volume by MRI-guided HIFU exposure under the irradiation power of 150 $W cm^{-2}$ and duration of 5 s in rabbit liver tumors after different agents were applied through the ear vein (inset: digital pictures of tumor tissue after HIFU exposure).

CAs. Then the ultrasonic transducer launches numerous low-energy ultrasound waves, which are focused on the targeted tissue in vivo to generate the transient high temperature to ablate the targeted tumor cells using MCNCs as the SAs. To assess the in vivo efficiency of PFH-encapsulated MCNCs as both the CAs and SAs for MRI-guided HIFU cancer surgery, the nanocapsules were intravenously administrated through the ear vein into rabbits bearing tumors in the liver. The MCNCs could be delivered into the tumors in the liver by phagocytosis of the nanoparticles by the RES and by EPR effects. After the administration of MCNCs/PBS and PFH-MCNCs/PBS for 30 min, the tumor could be distinguished clearly upon the MRI guidance (Figure 2), by which the ultrasound could be precisely focused on the desired tumor location. The T_1-weighted MRI signal intensities of the tumor part increase with prolonged time, further demonstrating that PFH-MCNCs could enter the tumor tissue (Figure 3c). After the exposure to focused ultrasound in tumors (150 W, 5 s), the rabbits were immediately anatomized to calculate the damaged volume in the tumor part. The mean volume of coagulated tumor by HIFU exposure in the rabbit that received PFH-MCNCs/PBS (10.2 mm^3) is 8.3 and 1.8 times larger than in the rabbits that received PBS (1.1 mm^3) and MCNCs/PBS (3.7 mm^3), respectively (Figure 3d). This finding demonstrates the high in vivo synergistic efficiency of the composite nanoparticles for MRI-guided HIFU cancer surgery, which is consistent with the results from the ex vivo bovine liver assessment. Pathological examinations of related tumor tissues (hematoxylin–eosin staining) after HIFU ablation revealed that the highly compact and aggregated tumor tissues stayed intact, and only a few denatured cells can be found upon HIFU exposure after the intravenous administration of PBS or MCNCs/PBS (Figure S7a, b in the Supporting Information). However, remarkably destructed cells, large vacuoles, and irregular widening of tumor tissues can be found in the tumor tissue that intravenously received PFH-MCNCs/PBS (Figure S7c, d in the Supporting Information), further demonstrating that PFH-MCNCs could bring forth the significant synergistic therapeutic effect for cancer surgery. It was anticipated that the PFH in MCNCs was gasified into bubbles under the high temperature caused by HIFU. This bubble formation oscillates with focused ultrasound and causes the formation of cavities, which results in the significant synergistic effect for HIFU ablation.[13] Impor-

tantly, HIFU could be precisely focused on the tumor with the help of MCNCs in MRI guidance, thus leaving the normal tissue undamaged and causing very low side effects.

In summary, we have introduced nano-biotechnology into non-invasive and non-radiative cancer therapy by using elaborately designed manganese-based multifunctional mesoporous composite nanocapsules as both CAs and SAs for MRI-guided HIFU cancer surgery. The unique nanostructure of the designed MCNCs endows them with distinctive advantages for MRI-guided HIFU therapy: First, the paramagnetic mesoporous shell with highly dispersed manganese oxide species confined within the mesopores of the MCNCs makes them suitable as CAs for efficient T_1-weighted MR imaging for accurate HIFU guidance. Second, the encapsulation and delivery of PFH molecules in the large hollow interiors as well as the penetrable mesopores makes them suitable as SAs for active HIFU synergistic therapy. With the assistance of MCNCs, the focused ultrasound can be precisely located on the targeted tumor tissue in the liver of rabbits, and a greatly enhanced synergistic therapeutic effect has been achieved. It is anticipated that the unique but excellent nanostructure of MCNCs can be applied for the loading and delivery of various guest molecules, for example, chemotherapeutic agents, for future combined MRI-based diagnosis, thermal-responsive chemotherapy, and imaging-guided HIFU surgery of cancers.

Received: September 1, 2011
Published online: November 10, 2011

Keywords: high-intensity focused ultrasound · imaging agents · magnetic resonance imaging · mesoporous materials · nanotechnology

[1] a) J. E. Kennedy, G. R. ter Haar, D. Cranston, *Br. J. Radiol.* **2003**, *76*, 590; b) A. C. Schmitz, D. Gianfelice, B. L. Daniel, W. Mali, M. van den Bosch, *Eur. Radiol.* **2008**, *18*, 1431.

[2] M. R. Bailey, V. A. Khokhlova, O. A. Sapozhnikov, S. G. Kargl, L. A. Crum, *Acoust. Phys.* **2003**, *49*, 369.

[3] a) K. Hynynen, *Ultrasonics* **2010**, *50*, 221; b) P. E. Huber, J. W. Jenne, R. Rastert, I. Simiantonakis, H. P. Sinn, H. J. Strittmatter, D. von Fournier, M. F. Wannenmacher, J. Debus, *Cancer Res.* **2001**, *61*, 8441; c) K. Hynynen, A. Darkazanli, E. Unger, J. F. Schenck, *Med. Phys.* **1993**, *20*, 107.

[4] a) N. K. Logothetis, *Nature* **2008**, *453*, 869; b) Y. W. Jun, J. H. Lee, J. Cheon, *Angew. Chem.* **2008**, *120*, 5200; *Angew. Chem. Int. Ed.* **2008**, *47*, 5122; c) E. Terreno, D. D. Castelli, A. Viale, S. Aime, *Chem. Rev.* **2010**, *110*, 3019; d) Y. Chen et al., *Adv. Funct. Mater.* **2011**, *21*, 270, see the Supporting Information.

[5] a) J. G. Penfield, R. F. Reilly, *Nat. Clin. Pract. Nephrol.* **2007**, *3*, 654–668; b) J. Perez-Rodriguez, S. Lai, B. D. Ehst, D. M. Fine, D. A. Bluemke, *Radiology* **2009**, *250*, 371; c) U. I. Tromsdorf, O. T. Bruns, S. C. Salmen, U. Beisiegel, H. Weller, *Nano Lett.* **2009**, *9*, 4434.

[6] a) Y. Chen, H. R. Chen, L. M. Guo, Q. J. He, F. Chen, J. Zhou, J. W. Feng, J. L. Shi, *ACS Nano* **2010**, *4*, 529; b) Y. Chen, H. R. Chen, D. P. Zeng, Y. B. Tian, F. Chen, J. W. Feng, J. L. Shi, *ACS Nano* **2010**, *4*, 6001; c) X. L. Fang, C. Chen, Z. H. Liu, P. X. Liu, N. F. Zheng, *Nanoscale* **2011**, *3*, 1632.

[7] K. M. L. Taylor, J. S. Kim, W. J. Rieter, H. An, W. L. Lin, W. B. Lin, *J. Am. Chem. Soc.* **2008**, *130*, 2154.

[8] Y. Chen, H. R. Chen, M. Ma, F. Chen, L. M. Guo, L. X. Zhang, J. L. Shi, *J. Mater. Chem.* **2011**, *21*, 5290.

[9] H. B. Na et al., *Angew. Chem.* **2007**, *119*, 5493; *Angew. Chem. Int. Ed.* **2007**, *46*, 5397, see the Supporting Information.

[10] a) H. Yang, Y. M. Zhuang, H. Hu, X. X. Du, C. X. Zhang, X. Y. Shi, H. X. Wu, S. P. Yang, *Adv. Funct. Mater.* **2010**, *20*, 1733; b) T. Kim et al., *J. Am. Chem. Soc.* **2011**, *133*, 2955, see the Supporting Information; c) Y. K. Peng et al., *ACS Nano* **2011**, *5*, 4177, see the Supporting Information.

[11] H. Maeda, J. Wu, T. Sawa, Y. Matsumura, K. Hori, *J. Controlled Release* **2000**, *65*, 271.

[12] E. G. Schutt, D. H. Klein, R. M. Mattrey, J. G. Riess, *Angew. Chem.* **2003**, *115*, 3336; *Angew. Chem. Int. Ed.* **2003**, *42*, 3218.

[13] a) Y. Kaneko, T. Maruyama, K. Takegami, T. Watanabe, H. Mitsui, K. Hanajiri, H. A. Nagawa, Y. Matsumoto, *Eur. Radiol.* **2005**, *15*, 1415; b) K. Takegami, Y. Kaneko, T. Watanabe, S. Watanabe, T. Maruyama, Y. Matsumoto, H. Nagawa, *Radiology* **2005**, *237*, 132.

